

Article

Enhancement in the Performance of Dye Sensitized Solar Cells (DSSCs) by Incorporation of Reduced Graphene Oxide (RGO) and Carbon Nanotubes (CNTs) in ZnO Nanostructures

Ahmed Alshahrie ^{1,2}, Ahmed A. Alghamdi ¹, Prince M. Z. Hasan ^{2,*}, Faheem Ahmed ³ ,
Hanadi Mohammed Eid Albalawi ³, Ahmad Umar ^{4,5,*}  and Abdullah Alsulami ⁶ 

¹ Department of Physics, faculty of Science, King Abdulaziz University, P.O. Box 80200, Jeddah 21589, Saudi Arabia

² Center of Nanotechnology, King Abdulaziz University, P.O. Box 80200, Jeddah 21589, Saudi Arabia

³ Department of Physics, College of Science, King Faisal University, P.O. Box-400, Al-Ahsa 31982, Saudi Arabia

⁴ Department of Chemistry, Faculty of Science and Arts and Promising Centre for Sensors and Electronic Devices (PCSED), Najran University, Najran 11001, Saudi Arabia

⁵ Department of Materials Science and Engineering, The Ohio State University, Columbus, OH 43210, USA

⁶ Physics Department, College of Sciences and Art at ArRass, Qassim University, ArRass 51921, Saudi Arabia

* Correspondence: prince.mufti@gmail.com (P.M.Z.H.); ahmadumar786@gmail.com (A.U.)

† Adjunct Professor at the Department of Materials Science and Engineering, The Ohio State University, Columbus, OH 43210, USA.



Citation: Alshahrie, A.; Alghamdi, A.A.; Hasan, P.M.Z.; Ahmed, F.; Albalawi, H.M.E.; Umar, A.; Alsulami, A. Enhancement in the Performance of Dye Sensitized Solar Cells (DSSCs) by Incorporation of Reduced Graphene Oxide (RGO) and Carbon Nanotubes (CNTs) in ZnO Nanostructures. *Inorganics* **2022**, *10*, 204. <https://doi.org/10.3390/inorganics10110204>

Academic Editors: Fan Zhang and Yanhong Lu

Received: 8 October 2022

Accepted: 9 November 2022

Published: 11 November 2022

Publisher's Note: MDPI stays neutral with regard to jurisdictional claims in published maps and institutional affiliations.



Copyright: © 2022 by the authors. Licensee MDPI, Basel, Switzerland. This article is an open access article distributed under the terms and conditions of the Creative Commons Attribution (CC BY) license (<https://creativecommons.org/licenses/by/4.0/>).

Abstract: In this work, a fast, environment-friendly and economic route was used to prepare ZnO and their nanocomposites containing reduced graphene oxide (RGO) and carbon nanotubes (CNTs) for the fabrication of dye-sensitized solar cells (DSSCs). The prepared nanostructures were well-characterized by X-ray diffraction (XRD), field emission scanning electron microscopy (FESEM), transmission electron microscopy (TEM), and Raman measurements. The XRD, Raman and TEM results confirmed that the ZnO nanostructures were crystallized into the hexagonal phase, and the nanocomposites containing RGO and CNTs. Morphological studies performed by using FESEM and TEM images showed that the ZnO possessed tube-like morphology with length and diameter in the range of ~1 micron and 90–200 nm, respectively, which were uniform and densely covered on the surface of the carbon materials. The DSSCs were fabricated using prepared nanostructures as a working electrode and platinum as a counter electrode with ruthenium-based dyes and iodide electrolytes. To further improve the efficiency of fabricated solar cells, nanocomposites of prepared nanostructures of ZnO with RGO and CNTs were synthesized, and their results were compared with the pristine samples. The results showed that the ZnO/CNTs (0.5 wt%) nanocomposites electrode exhibited the highest power conversion efficiency (PCE) of DSSCs with a maximum value of 0.612% compared to 0.326% of DSSC with pure ZnO, and 0.574% of DSSC with ZnO/RGO. Significantly, this technique could be used for large-scale production using the existing economical and highly effective DSSC fabrication technique.

Keywords: ZnO; graphene oxide; DSSCs; power conversion efficiency

1. Introduction

Dye-sensitized solar cells (DSSC) have emerged as cost-effective alternatives to thin-film solar cells [1]. In the fight for high efficiency at a low cost, dye-sensitized solar cells are a serious rival. Because of their low cost, compatibility with flexible materials, and ability to improve the specific parts, DSSCs have inspired a lot of research interest [2]. Unlike semiconductor junction-based solar cells, essential operations of DSSCs, such as light absorption, electron transport, and hole transport, are carried out by different materials, allowing each material to be adjusted separately for the best performance [2]. Generally, the basic principle of DSSCs is very similar to the naturally occurring photosynthesis wherein

various dyes are combined on a large bandgap of semiconducting nanomaterials and deposited on the conducting ITO substrate that initiates the energy conversion process [3]. The photoanode in the sunlight and the excited states of the dye inject electrons into the conduction band of the semiconducting nanomaterials, which are quickly transported to the counter electrode. Meanwhile, the original state of the dye molecules is returned by the electron donation from the iodide-based redox electrolyte. Recently, researchers have been focused on developing low-cost counter electrodes, fast electron transport semiconductor photoanodes and natural dyes [3,4].

Commonly, many wide bandgap semiconductors have been used as photoanodes for DSSC devices, such as zinc oxide (ZnO), niobium pentoxide (Nb₂O₅), tin dioxide (SnO₂), and titanium dioxide (TiO₂) nanoparticles [5–13]. Among these semiconducting nanomaterials, ZnO is considered as an efficient photoanode because of its high ability to endure constant electron transfer under sun light irradiation in the visible to ultraviolet range [5–8]. ZnO shows high mobility of the order of 100 cm²/V s and is considered a potential substitute for the TiO₂ due to their similar band gaps and electron affinities [8–10,13–15]. An important advantage of ZnO over TiO₂ is that it can be synthesized by applying a wide range of synthesis techniques to obtain a great variety of different morphologies and nano-structured electrodes. The nano-structured morphologies of ZnO have a high surface area that enhances the dye absorption over photo-anodes. However, the energy conversion efficiency of ZnO-based cells is typically not as high as required. Therefore, there is considerable interest in further improving the efficiency of ZnO-based cells by altering the morphology of a ZnO photo-anode to achieve a higher surface area and efficient charge transport. It is well-known that the morphology of ZnO can alter various functional properties, which makes them useful in various applications. Previous work reported the effects of reaction time on the morphological, structural, and gas/chemical-sensing properties of ZnO nanostructures [16–23]. In another work, the authors reported the surfactant dependent growth of twinned ZnO nanodisks [18].

Additionally, a nanocomposite-based photoanode of ZnO and carbon could lead to an improvement in the performance of DSSCs. Among the various nanocomposite materials, carbon-based materials including graphene and carbon nanotubes [20–25] have been proposed as an additive material for ZnO photoanodes to increase electron mobility, owing to their outstanding electronic properties. It has an excellent mobility of charge carrier (200,000 cm²V⁻¹s⁻¹) [21] and a large specific surface area (2630 m²/g) [22].

In this work, a fast and cost-effective route for the growth of ZnO nanostructures and their carbon-based (RGO and CNTs) nanocomposites was reported to fabricate the DSSCs using ZnO/RGO- and ZnO/CNTs-based photoanodes. An investigation on the effect of RGO and CNTs on the performance of DSSCs was studied, and the results of pure ZnO-based DSSCs were compared. It was observed that the incorporation of carbon-based materials into ZnO improved the performance of DSSCs more so than that of pure ZnO nanostructures. More specifically, nanocomposites of ZnO/CNTs deliver higher efficiency and enhanced performance compared to the nanocomposites of ZnO/RGO.

2. Experimental Details

2.1. Preparation of Zinc Oxide (ZnO)

To prepare ZnO by the soft chemical route, 0.03 M of sodium hydroxide (NaOH) was dissolved in 84 mL of ethanol and heated for 2 h on a hot plate at 70 °C. After the heating, 0.01 M zinc acetate dissolved in 125 mL ethanol was prepared and slowly added to NaOH solution and continuously stirred for 30 min. After homogeneous mixing, a 0.035 M solution of hexamethylenetetramine in 50 mL DI water was added to the 5 mL (NaOH and Zinc acetate) solution, which was preheated at 85 °C. In this solution, 5 mL zinc nitrate solution with 5 mL DI water was added and the heating was continuous for 2 h and maintained at 85 °C and 95 °C. The samples were washed thoroughly with ethanol and DI water several times and finally dried at 80 °C for 24 h.

2.2. Preparation of Graphene Oxide (GO)

The graphite was oxidized using Hummer's method to produce the GO. For the preparation, 3.5 g of graphite was mixed vigorously with 100 mL of 98% H₂SO₄ in a 100 mL flask. A total of 10 g of KMNO₄ was added at a temperature of less than 20 °C. The mixture was transferred to 500 mL of deionized water after 2 h of stirring at 35 °C, and 20 mL of 30% H₂SO₄ was added to remove any excess permanganate. The suspension turned bright yellow after being exposed to peroxide. Filtration through a sintered glass filter was used to purify the GO. The filtrate was washed in HCl before being washed in hot water to remove any remaining sulfate ions, resulting in a yellowish-brown filter cake. After repeated washings with hot water, the final GO preparation was dried at 80 °C.

2.3. Preparation of Reduced Graphene Oxide (RGO)

After 30 min of ultrasonic treatment, GO was dispersed in DI water. As a result, a brown GO aqueous suspension that was homogeneous was obtained. The suspension's pH was raised to 10 by removing NH₃H₂O. Amounts of hydrazine hydrate were added to the suspension and heated at 80 °C for 24 h, with a 10:7 weight ratio of hydrazine hydrate to GO. The solution gradually precipitated a kind of black flocculent substance. The product was obtained after it was filtered through a high-quality filter paper. Finally, the black product was washed in methanol and water before being dried at 80 °C for 24 h.

2.4. Growth of CNTs by CVD Method

For the growth of the CNTs, a Si/SiO₂ substrate was used in the present experiment. The cleaning process of the substrate was carried out before the growth. During the cleaning, the substrate was cleaned by using deionized water (DI water) and ethanol several times followed by air drying the substrate. The substrate was placed in a DC-sputtering system, and ~25 nm of a Ni catalyst layer was deposited on its surface. In addition, a Cr layer of ~5 nm, an electrically conductive thin barrier layer between the substrates and the Ni catalyst layer, was deposited. After this step, the growth of the MWCNTs was achieved by using plasma enhanced chemical vapor deposition (PECVD) in an EasyTube 3000 (First-Nano; South Technology Drive, Central Islip, NY, USA) system. At the end of the growth period, the samples were slowly cooled, within the furnace, under a H₂ gas environment. The CNTs obtained were carefully scratched from the substrate and used to make nanocomposites.

2.5. Preparation of Nanocomposites of ZnO, RGO and CNTs

The composites of the prepared ZnO with RGO and CNTs have been prepared in a weight ratio of 0.5%. The required amount of RGO and CNTs was mixed during the growth of ZnO nanostructures by wet chemical reaction. The final product as nanocomposites was washed thoroughly following similar steps and dried at 80 °C for 24 h.

2.6. Fabrication of Dye-Sensitized Solar Cells (DSSC)

The fabrication of DSSCs was performed using ITO (indium doped tin oxide)-coated glass substrates as conducting substrates. Different samples of ZnO, ZnO/RGO, and ZnO/CNTs were used as working electrodes. Slurry of the working electrode was prepared under ambient conditions with the help of agate mortar followed by adding ethanol to avoid aggregation and drops of Triton X100 as a surfactant to maintain smoothness in the paste. The composite paste was then cast by a doctor-blade method on a cleaned and dried ITO conductive glass substrate. The coated glass substrate was annealed at 550 °C for 1 h. The electrodes were soaked in the dye solution (N719) for 24 h. After sensitization, the samples were washed with ethanol to eliminate unanchored dye. Another ITO-coated glass was used to make the counter electrode, and on its conductive side, a thin layer of Pt solution was deposited. Both the electrodes were placed upside down such that the nanomaterials layer and Pt layer were contacted with each other with the binder clips to complete the DSSC assembly. A liquid electrolyte (iodide/triiodide)-based solution was

placed at the top of the conductive edge of the cell. This liquid electrolyte was put into the space between the two conductive electrodes with capillary action. The effective cell surface area was 1 cm^2 .

2.7. Characterizations

The X-ray diffraction (XRD) patterns in the range of $20\text{--}80^\circ$ were recorded by a MiniFlex600 (Rigaku, Tokyo, Japan) X-ray diffractometer using $\text{Cu-K}\alpha$ radiation (wavelength = 1.5406 \AA). A morphological study of the product was performed using transmission electron microscopy (TEM; Model: JEOL JEM-2100F) at 200 kV and scanning electron microscopy (SEM) using (JSM-7610F, JEOL, Tokyo, Japan). Raman spectroscopy studies were carried out using a confocal Raman microscope (LabRAM, HR800, Longjumeau, France SAS). A solar simulator system was used to measure the I–V characteristics of the DSSCs under the illumination of one sun (AM 1.5G) (100 mW/cm^2).

3. Result and Discussion

XRD patterns of ZnO samples synthesized at 85 and 95°C via a soft chemical route are shown in Figure 1. The XRD patterns show a single-phase nature with the hexagonal wurtzite structure for ZnO samples as indexed using POWDER-X software (beta version) (JCPDS, 36-1451), and no indication of the secondary phase can be seen. An increase in the peak intensity with the increase in the temperature of ZnO samples was observed. This increase in peak intensity could be attributed to the fact that the increase in temperature increases the crystallite size of the ZnO samples. In order to see the effect of the addition of a carbon phase in ZnO, Figures 2 and 3 show the XRD patterns of ZnO/RGO and ZnO/CNTs, respectively. It is clear from the figures that all of the characteristic peaks of ZnO are well maintained at the designated position; however, there are some additional peaks that belong to the RGO and CNTs, as shown in Figures 2 and 3. The findings revealed the formation of nanocomposites of ZnO with the RGO and CNTs.

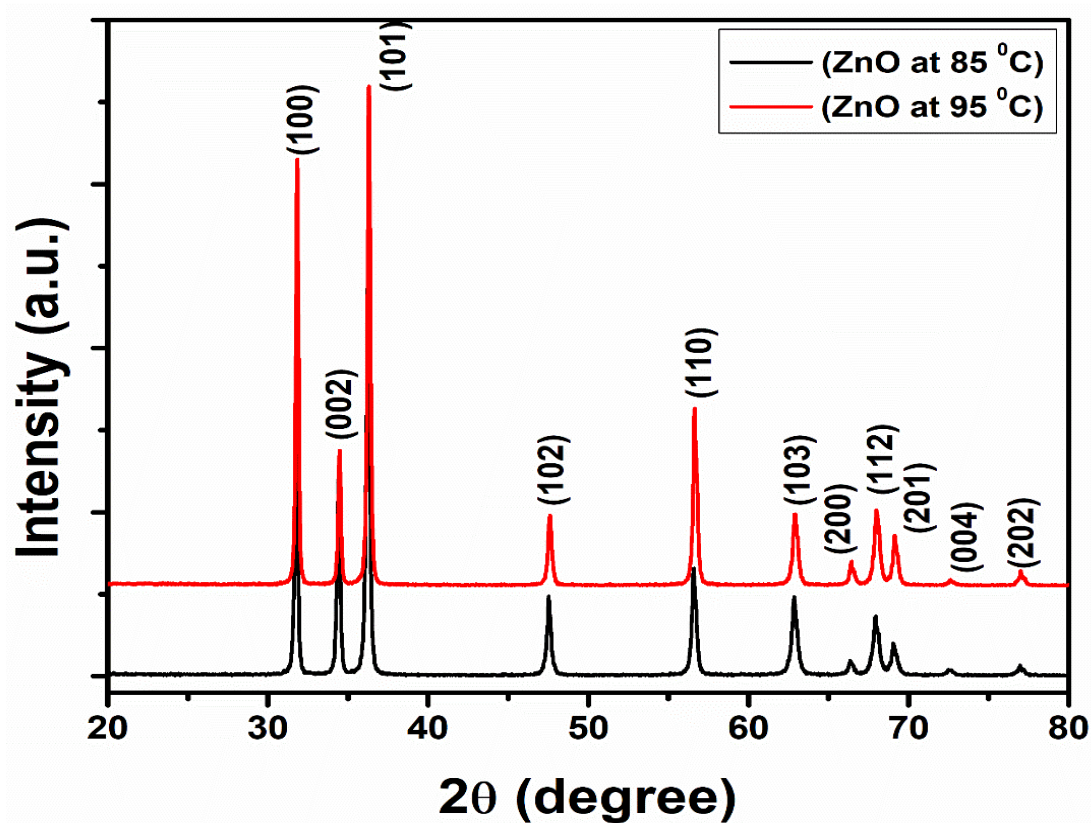


Figure 1. XRD patterns of ZnO prepared at different temperatures.

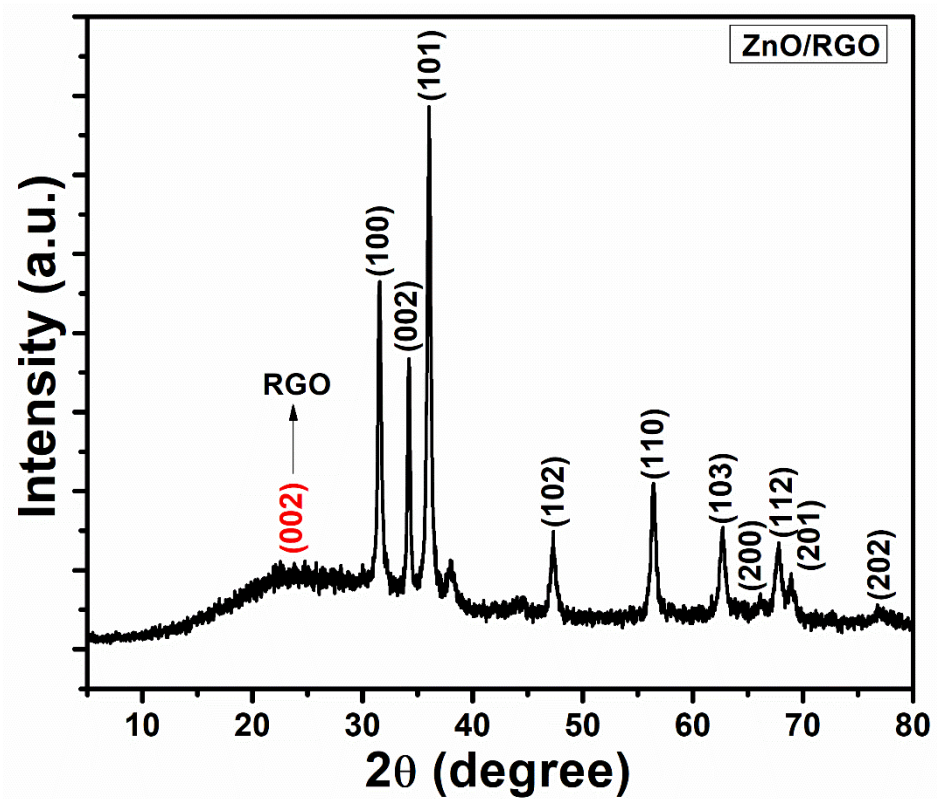


Figure 2. XRD patterns of ZnO/RGO nanocomposites.

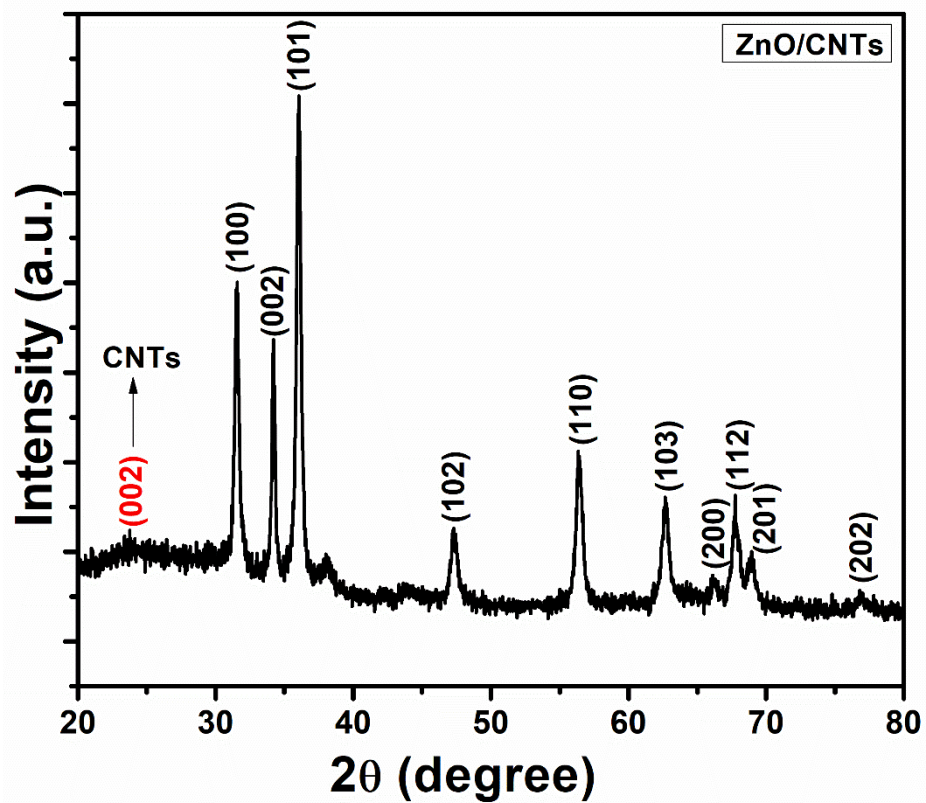


Figure 3. XRD patterns of ZnO/CNTs nanocomposites.

The Raman spectra are sensitive to the crystal quality, structural defects and disorders of the grown products. ZnO has a Wurtzite structure that belongs to the C_{6v} symmetry

group. Figure 4a shows the Raman spectra of ZnO samples prepared at 85 °C, and Figure 4b shows the Raman spectrum of ZnO/RGO nanocomposites. The Raman mode for the as-prepared pure ZnO samples is in good agreement with the characteristic peak of ZnO. In contrast, several changes in the Raman mode can be observed for ZnO/RGO samples. As can be seen in Figure 4a, the most prominent mode for pure ZnO is E₂ high at ~438 cm⁻¹, which is attributed to the vibration of oxygen atoms [25]. However, an increase in peak intensity with a blue shift towards 435 cm⁻¹ is observed in the Raman spectrum for ZnO/RGO, as shown in Figure 4b. This increase and shift in the peak intensity could be due to the varying defect structure owing to mechanical activation. In addition to the characteristic features of ZnO, D and G bands appeared at ~1340 and 1580 cm⁻¹, respectively. These D and G bands are the characteristic peaks of RGO or carbon material. This indicates that the RGO has been successfully incorporated with ZnO.

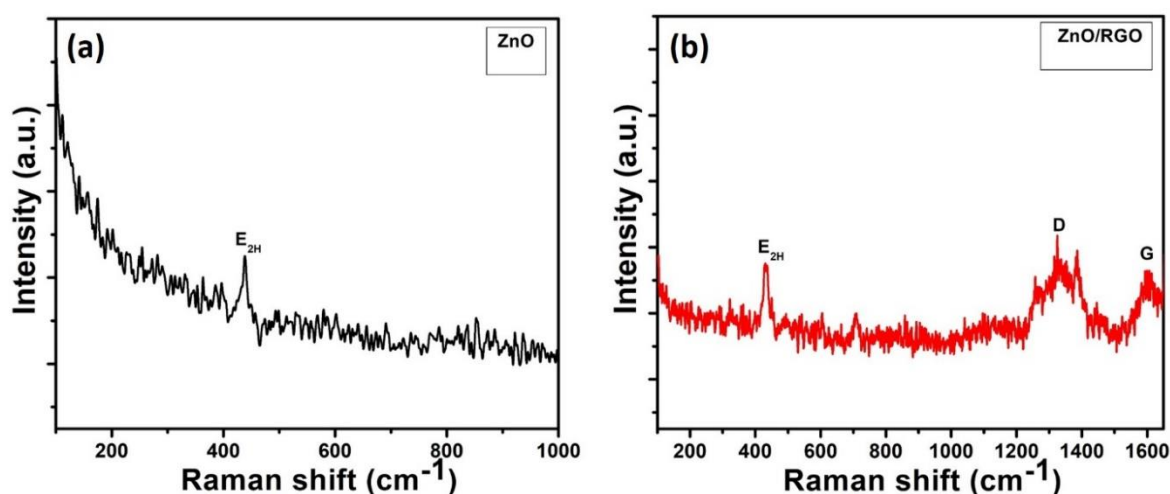


Figure 4. Raman spectra of (a) ZnO and (b) ZnO/RGO nanocomposites.

Figure 5 shows the FESEM image of ZnO samples prepared at two different temperatures of 85 and 95 °C. It is clear from Figure 5a,b that the nanotube-like morphology could be seen with an average length of a few microns and a diameter in the range of 80–200 nm. These nanotubes show clear openings, which are produced at a temperature of 85 °C. When the temperature of the reaction was increased to 95 °C, one can observe that the nanotube's morphology transformed to the aggregates, which are made up of ZnO nanosheets (c–d). The thickness and lateral dimension of the ZnO nanosheets are ~30 and ~400 nm, respectively.

Additional morphological features and the crystalline quality of ZnO nanotubes were achieved through TEM analysis. Figure 6a shows the TEM image of a single nanotube with length and diameter in the range of ~1 micron and 90–200 nm, respectively. The atomic structure-related information obtained from the HRTEM image in Figure 6b depicts the highly crystalline nature of ZnO nanotubes with the interlayer spacing of 0.265 nm, which attributes to the d spacing of (002) lattice plane in ZnO structures. The results that were obtained from HRTEM further confirm the XRD studies where the ZnO nanotubes have preferred growth direction along the c-axis. The EDX spectrum of ZnO nanotubes clearly shows Zn and O peaks (Figure 6c), with no evidence for the presence of any other impurity peak.

Figure 7a shows the TEM image of nanocomposites with the incorporation of RGO in ZnO, where the nanotubes are wrapped with RGO sheets and few of these nanotubes are anchored on the surface of RGO sheets. Elemental studies, as shown in Figure 7b, depict the signals of Zn, O, and C, which further confirm the nanocomposites of ZnO and RGO.

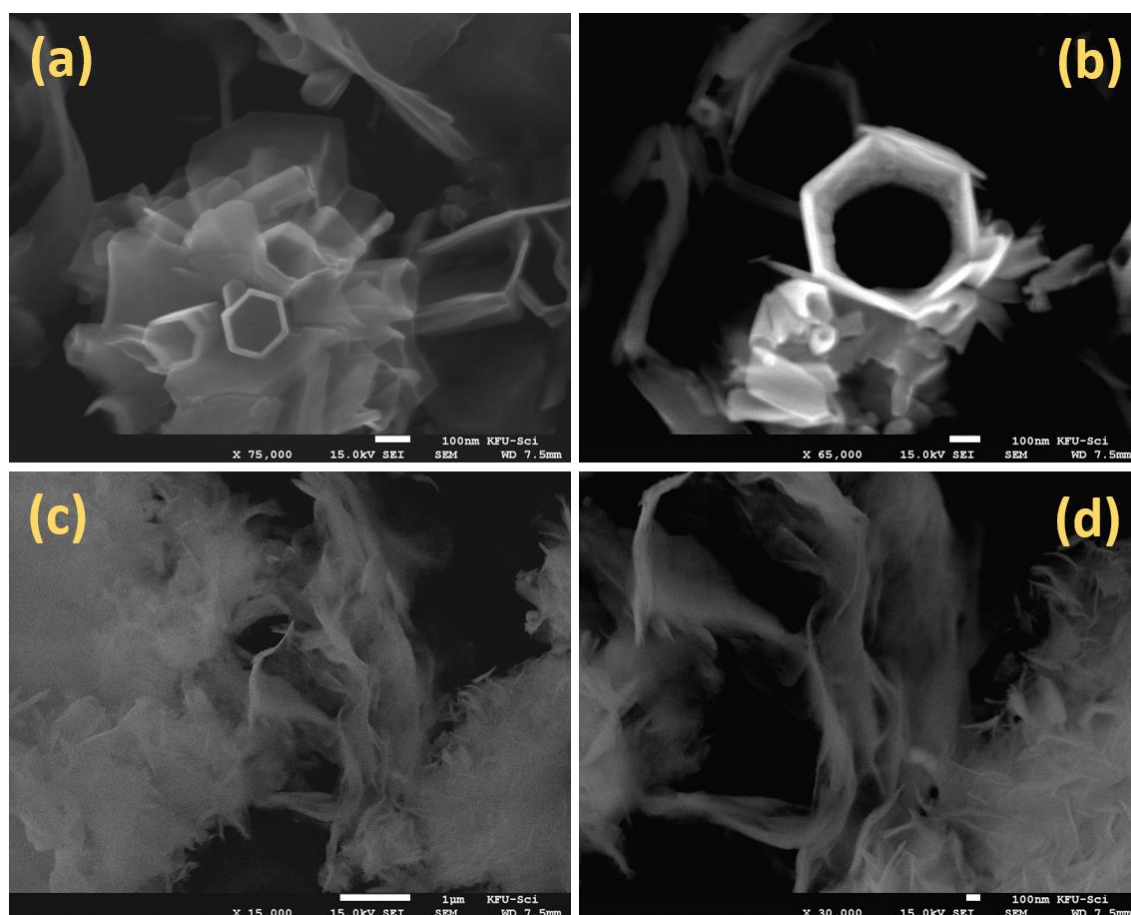


Figure 5. FESEM images of ZnO prepared at (a,b) 85 °C and (c,d) 95 °C.

The current density–voltage (J–V) curves with the pure ZnO and a weight ratio of 0.5 wt.% of RGO and CNTs incorporated in the ZnO are shown in Figure 8, and their photovoltaic parameters such as short-circuit current density (J_{sc}), open circuit voltage (V_{oc}), fill factor (FF), and photovoltaic conversion efficiency (η) are summarized in Table 1. The performance of ZnO nanostructure-based DSSCs was compared with the ZnO/RGO and ZnO/CNTs nanocomposite-based DSSCs. Figure 8 and Table 1 clearly reveal that ZnO shows a characteristic of DSSCs having a current density J_{sc} of 0.20 mA cm^{-2} . However, ZnO/RGO nanocomposites show an increase in current density to 0.24 mA cm^{-2} , while a slight decrease in the current density (0.22 mA cm^{-2}) was observed for the ZnO/CNTs nanocomposites.

Table 1. Summarized table of DSSCs parameters for samples of ZnO and their nanocomposites.

Samples	V_{oc} (V)	J_{sc} (mA/cm^2)	FF %	Efficiency (η) (%)
ZnO (85 °C)	0.43	0.202	38.37	0.326
ZnO/RGO (0.5%)	0.46	0.241	52.21	0.574
ZnO/CNTs (0.5%)	0.48	0.220	58.10	0.612

Additionally, the ZnO/CNTs device shows the highest efficiency of 0.61%, having a V_{oc} of 0.48 V, J_{sc} of 0.22 mA cm^{-2} and FF of 58.10%, which is almost double the efficiency attained by the pure ZnO-based DSSCs (~0.326%). However, ZnO/RGO-based DSSCs produce a slightly lower efficiency of 0.574%, with a V_{oc} of 0.46 V, J_{sc} of 0.24 mA cm^{-2} and FF of 52.21%. The obtained efficiencies of ZnO/RGO and ZnO/CNTs are much higher than that of pure ZnO.

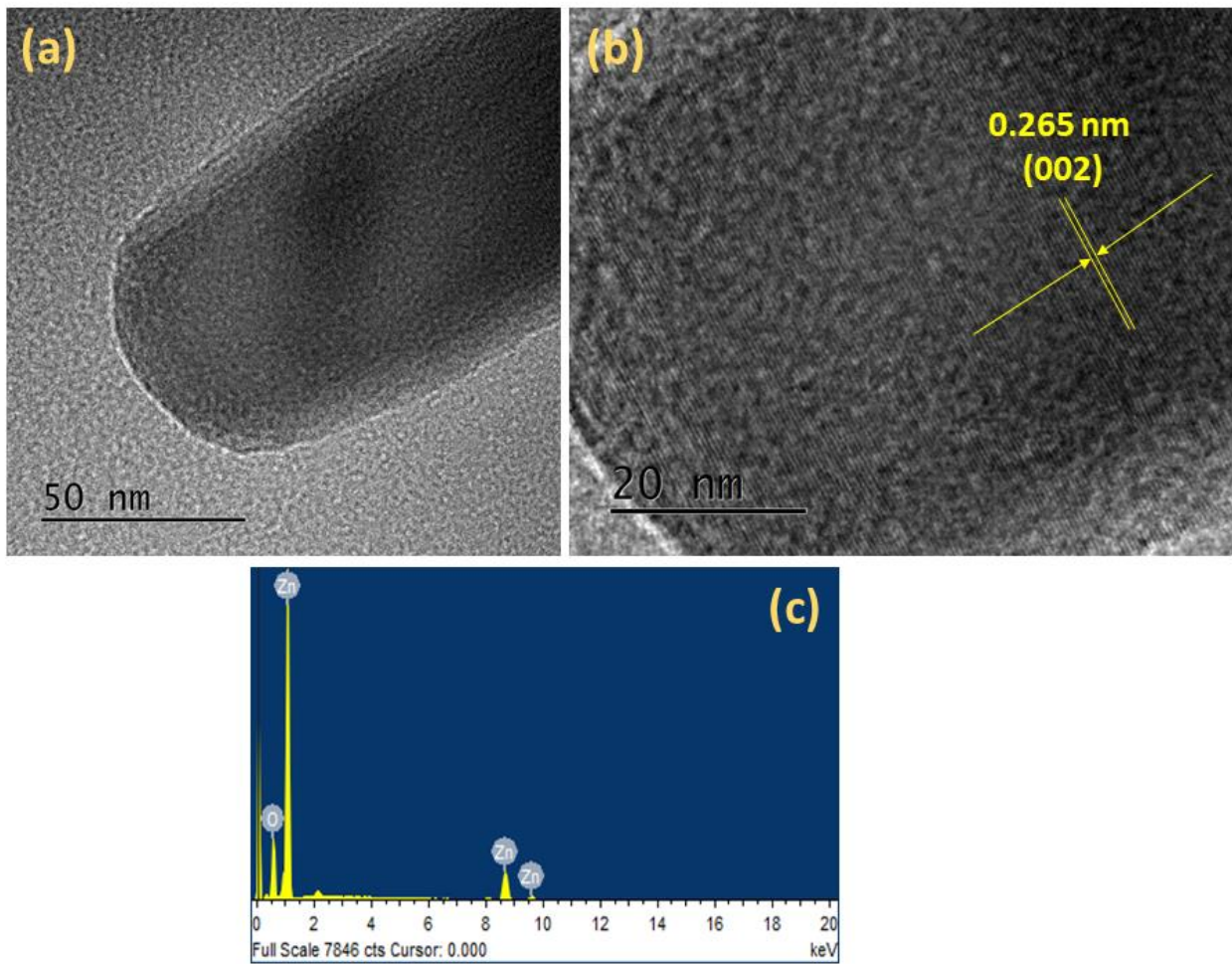


Figure 6. (a) TEM image, (b) HRTEM image, and (c) EDX spectrum of ZnO prepared at 85 °C.

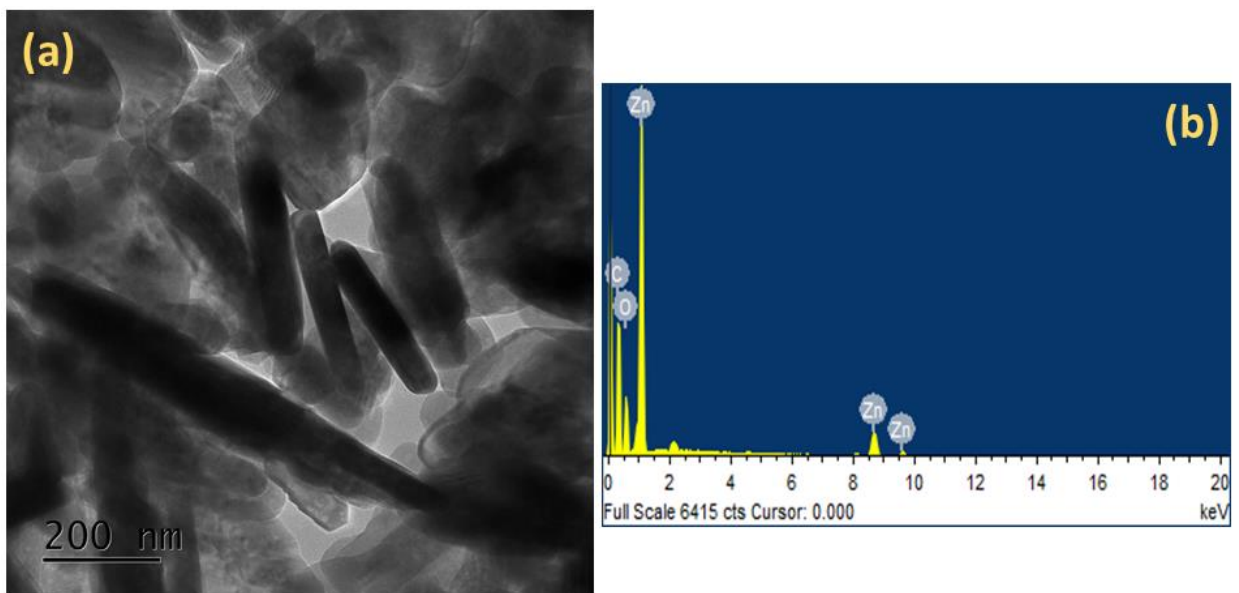


Figure 7. (a) TEM image, and (b) EDX spectrum of ZnO/RGO nanocomposites.

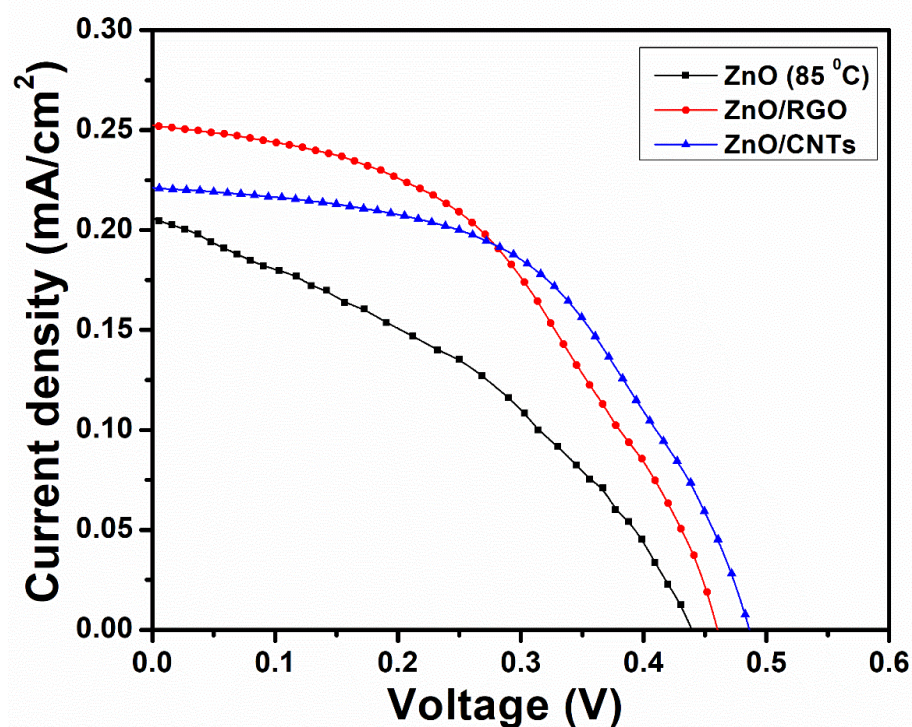


Figure 8. Current density–voltage (J–V) curves of ZnO nanocomposites.

4. Conclusions

In summary, a fast, cost-effective, and highly reproducible methodology of using soft chemicals to fabricate ZnO nanostructures and their RGO and CNTs nanocomposite-based DSSCs has been presented. The nanocomposites of ZnO were well characterized by using XRD, FESEM, TEM, and Raman spectroscopy measurements. A systematic investigation with the incorporation of 0.5 wt% RGO and CNTs in ZnO has been performed, and the effect of carbon materials on the performance of DSSCs has been observed. The incorporation of RGO and CNTs in ZnO is slowing down the recombination of photogenerated electrons, extending the excitation wavelength and increasing the surface-adsorbed amount of dye. It was observed that the dispersion of small amounts of RGO and CNTs (0.5 wt%) in ZnO can significantly improve the photo conversion efficiency of DSSCs. The optimum concentration of 0.5 wt% of CNTs in the ZnO photoanode did not affect the transparency of the ZnO layer but significantly increased the PCE of DSSC, with a maximum value of 0.612% compared to 0.326% of pure ZnO-based DSSC, and 0.574% for ZnO/RGO-based DSSC. This enhancement in the performance of CNTs and RGO-based ZnO DSSC could be due to the improved dye loading and electronic conductivity of photogenerated charge carriers and also the prevention of the electron–hole pair recombination process.

Author Contributions: Conceptualization, F.A., P.M.Z.H., A.U. and A.A. (Ahmed Alshahrie); methodology, F.A. and H.M.E.A.; validation, A.U. and A.A.A.; formal analysis, F.A. and H.M.E.A.; investigation, A.U. and A.A.A.; resources, A.A. (Abdullah Alsulami) and A.A.A.; data curation, F.A. and P.M.Z.H.; writing—original draft preparation, F.A., A.U. and H.M.E.A.; writing—review and editing, F.A. and A.U.; funding acquisition, A.A. (Abdullah Alsulami) and A.A.A. All authors have read and agreed to the published version of the manuscript.

Funding: This research was funded by deanship of scientific research (DSR) at King Abdulaziz University, Jeddah, Saudi Arabia, under grant number (RG-62-13-38).

Data Availability Statement: Available on request.

Acknowledgments: This project was funded by the deanship of scientific research (DSR) at King Abdulaziz University, Jeddah, Saudi Arabia, under grant number (RG-62-13-38). The authors, therefore, acknowledge with thanks DSR for technical and financial support.

Conflicts of Interest: The authors declare no conflict of interest.

References

1. Hardin, B.E.; Snaith, H.J.; McGehee, M.D. The renaissance of dye-sensitized solar cells. *Nat. Photonics*. **2012**, *6*, 162–169. [[CrossRef](#)]
2. Babar, F.; Mehmood, U.; Asghar, H.; Mehdi, M.H.; Khan, A.U.H.; Khalid, H.; Huda, N.U.; Fatima, Z. Nanostructured photoanode materials and their deposition methods for efficient and economical third generation dye-sensitized solar cells: A comprehensive review. *Energy Rev.* **2020**, *129*, 109919. [[CrossRef](#)]
3. Bella, F.; Gerbaldi, C.; Barolo, C.; Grätzel, M. Aqueous dye-sensitized solar cells. *Chem. Soc. Rev.* **2015**, *44*, 3431–3473. [[CrossRef](#)] [[PubMed](#)]
4. Peter, L.M. Dye-sensitized nanocrystalline solar cells. *Phys. Chem. Chem. Phys.* **2007**, *9*, 2630–2642. [[CrossRef](#)]
5. Won, S.; Kim, J.S. Spinach Extract Derived Carbon Dots Decorated on ZnO Nanorods for Photocatalytic Dye Degradation. *Sci. Adv. Mater.* **2021**, *13*, 922–926. [[CrossRef](#)]
6. Yu, J.; Kim, J. Synthesis and Characterization of ZnO Doped with Gold Nanoparticles for Improved Photocatalytic Activity. *Sci. Adv. Mater.* **2021**, *13*, 944–948. [[CrossRef](#)]
7. Chang, G.J.; Lin, S.Y.; Wu, J.J. Room-temperature chemical integration of ZnO nanoarchitectures on plastic substrates for flexible dye-sensitized solar cells. *Nanoscale* **2014**, *6*, 1329–1334. [[CrossRef](#)]
8. Barpuzary, D.; Patra, A.S.; Vaghasiya, J.V.; Solanki, B.G.; Soni, S.S.; Qureshi, M. Highly efficient one-dimensional ZnO nanowire-based dye-sensitized solar cell using a metal-free, D- π -A-type, carbazole derivative with more than 5% power conversion. *ACS Appl. Mater. Interfaces* **2014**, *6*, 12629–12639. [[CrossRef](#)]
9. Umar, A.; Singh, J.; Ibrahim, A.A.; Kumar, R.; Rai, P.; Rai, A.K.; Algadi, H.; Alhamami, M.A.M.; Elsdidiq, M.M.E. Cauliflower-Shaped ZnO Nanostructure for Enhanced NO₂ Gas Sensor Application. *Sci. Adv. Mater.* **2021**, *13*, 2358–2363. [[CrossRef](#)]
10. Anta, J.A.; Guillén, E.; Tena-Zaera, R. ZnO-based dye-sensitized solar cells. *J. Phys. Chem. C* **2012**, *116*, 11413–11425. [[CrossRef](#)]
11. Hwang, J.Y.; Kim, I.T.; Choi, H.W. Characteristics of Perovskite Solar Cells with ZnGa₂O₄:Mn Phosphor Mixed Polyvinylidene Fluoride Down-Conversion Layer. *J. Nanoelectron. Optoelectron.* **2021**, *16*, 855–860. [[CrossRef](#)]
12. Umar, A.; Ibrahim, A.A.; Kumar, R.; Rana, K.; Algadi, H.; Alhamami, M.A.M.; Elsdidiq, M.M.E.; Mohammed, A.Y.A. Aluminum Doped ZnO Nanorods for Enhanced Phenylhydrazine Chemical Sensor Applications. *Sci. Adv. Mater.* **2021**, *13*, 2483–2488. [[CrossRef](#)]
13. Wei, M.; Konishi, Y.; Zhou, H.; Yanagida, M.; Sugihara, H.; Arakawa, H. Highly efficient dye-sensitized solar cells composed of mesoporous titanium dioxide. *J. Mater. Chem.* **2006**, *16*, 1287–1293. [[CrossRef](#)]
14. Wang, Y.Q.; Chen, S.G.; Tang, X.H.; Palchik, O.; Zaban, A.; Kolytyn, Y.; Gedanken, A. Mesoporous titanium dioxide: Sonochemical synthesis and application in dye-sensitized solar cells. *J. Mater. Chem.* **2001**, *11*, 521–526. [[CrossRef](#)]
15. Law, M.; Greene, L.E.; Johnson, J.C.; Saykally, R.; Yang, P. Nanowire dye-sensitized solar cells. *Nat. Mater.* **2005**, *4*, 455. [[CrossRef](#)] [[PubMed](#)]
16. Yoshida, T.; Terada, K.; Schlettwein, D.; Oekermann, T.; Sugiura, T.; Minoura, H. Electrochemical Self-Assembly of Nanoporous ZnO/Eosin Y Thin Films and Their Sensitized Photoelectrochemical Performance. *Adv. Mater.* **2000**, *12*, 1214. [[CrossRef](#)]
17. Hosono, E.; Fujihara, S.; Honma, I.; Zhou, H. Fabrication of morphology and crystal structure controlled nanorod and nanosheet cobalt hydroxide based on the difference of oxygen-solubility between water and methanol, and conversion into Co₃O₄. *Adv. Mater.* **2005**, *17*, 2091. [[CrossRef](#)]
18. Hussain, S.; Liu, T.; Kashif, M.; Lin, L.; Wu, S.; Guo, W.; Zeng, W.; Hashim, U. Effects of reaction time on the morphological, structural, and gas sensing properties of ZnO nanostructures. *Mater. Sci. Semicond. Process.* **2014**, *18*, 52–58. [[CrossRef](#)]
19. Ahmed, F.; Arshi, N.; Anwar, M.S.; Danisha, R.; Koo, B.H. Morphological evolution of ZnO nanostructures and their aspect ratio-induced enhancement in photocatalytic properties. *RSC Adv.* **2014**, *4*, 29249–29263.
20. Hussain, S.; Liu, T.; Kashif, M.; Miao, B.; He, J.; Zeng, W.; Zhang, Y.; Hashim, U.; Pan, F. Surfactant dependent growth of twinned ZnO nanodisks. *Mater. Lett.* **2014**, *118*, 165–168. [[CrossRef](#)]
21. Koumura, N.; Zhong-Sheng, W.; Mori, S.; Miyashita, M.; Suzuki, E.; Hara, K. Alkyl-functionalized organic dyes for efficient molecular photovoltaics. *J. Am. Chem. Soc.* **2006**, *128*, 14256–14257. [[CrossRef](#)] [[PubMed](#)]
22. Yang, N.; Zhai, J.; Wang, D.; Chen, Y.; Jiang, L. Two-dimensional graphene bridges enhanced photoinduced charge transport in dye-sensitized solar cells. *ACS Nano* **2010**, *4*, 887–894. [[CrossRef](#)] [[PubMed](#)]
23. Bolotin, K.I.; Sikes, K.J.; Jiang, Z.; Klima, M.; Fudenberg, G. Ultrahigh electron mobility in suspended graphene. *J. Hone Solid State Commun.* **2008**, *146*, 1–355. [[CrossRef](#)]
24. Stoller, M.D.; Park, S.; Zhu, Y.; An, J.; Ruoff, R.S. Graphene-based ultracapacitors. *Nano Lett.* **2008**, *8*, 3498. [[CrossRef](#)]
25. Alim, K.A.; Fonoberov, V.A.; Shamsa, M.; Balandin, A.A. Micro-Raman investigation of optical phonons in ZnO nanocrystals. *J. Appl. Phys.* **2005**, *97*, 124313. [[CrossRef](#)]